Scaling the electrical current switching of exchange bias in fully epitaxial antiferromagnet/ferromagnet bilayers

T. Hajiri [*], H. Goto, and H. Asano
Department of Materials Physics, Nagoya University, Nagoya 464-8603, Japan

While the electrical current manipulation of antiferromagnets (AFMs) has been demonstrated, the extent of the studied AFM materials has been limited with few systematic experiments and a poor understanding. We compare the electrical current switching of the exchange-bias field (H_{ex}) in AFM-Mn$_3A$N/ferromagnet-Co$_3$FeN bilayers. An applied pulse current can manipulate H_{ex} with respect to the current density and FM layer magnetization, which shifts exponentially as a function of the current density. We found that the saturation current density and exponential decay constant τ increase with the local moment of AFM Mn atoms. Our results highlight the effect of the AFM local moment to electrical current switching of H_{ex}, although it has a near-zero net magnetization, and may provide a facile way to explore the electrical current manipulation of AFM materials.

I. INTRODUCTION

Electrical manipulation of magnetic moments of ferromagnets (FMs) using spin-transfer torque (STT) and spin-orbit torque (SOT) has been widely studied towards spintronic applications [1–4]. Recently, antiferromagnetically coupled materials, such as ferrimagnets, synthetic antiferromagnets (AFMs), and AFMs, have attracted significant attention due to their promising potential in spintronic applications because of several properties, such as the absence of stray magnetic fields, terahertz spin dynamics, and stability against external perturbations [5–7]. The electrical current switching of the AFM Néel vector has been demonstrated for several AFM materials, such as CuMnAs [8,9], Mn$_2$Au [10,11], NiO [12–14], and Fe$_2$O$_3$ [15], with electrical current densities on the order of 10^7–10^8 A/cm^2, and recently switching with the order of 10^6 A/cm^2 has been realized on noncollinear AFM of Mn$_3$GaN [16] and Mn$_3$Sn [17]. In addition, the electrical current switching of ferrimagnets has been demonstrated. In particular, the magnetic moments of transition-metal (TM) and rare-earth (RE) ferrimagnets can be aligned in an antiparallel orientation, which enables tuning the magnetization around the compensation points by varying the relative constituent concentrations. The torque efficiency increases with divergent behaviors due to negative exchange interactions towards the compensation points [18,19]. On the other hand, in AFM, there are few systematical studies due to the difficulty of reading out the AFM Néel vector electrically as only a few AFM materials exhibit large electrical signals as an anomalous Hall effect [20–22] and anisotropic magnetoresistance [23–26].

To address this issue, we focused on the electrical switching of the exchange-bias field H_{ex}, which was first reported more than a decade ago [27,28]. The exchange-bias effect has

been widely studied because of its general use in spintronic devices, such as for spin-valve type magnetic memory [29,30]. In general, the exchange-bias effect occurs at the interfaces between FM and AFM materials, regardless of the material combination [31]. Therefore, in principle, electrical switching for H_{ex} can be adapted to all AFM materials. The early studies of electrical switching for H_{ex} demonstrated that spin torque can act not only on FM but also on AFM order parameters. Several related studies were conducted to further explore this observation [32–36]; however, no clear relationship was reported between the H_{ex} switching behavior and the electrical current density.

Based on theoretical studies of the electrical current switching of the AFM Néel vector in AFM/FM bilayers where the spin-polarized current is injected into the AFM through the FM layer, the critical current density i_c is expressed as

$$i_{c,\text{AFM}} = \frac{2\gamma_{\text{AFM}}\omega_{\text{AFM}}M_{\text{AFM}}d_{\text{AFM}}}{\gamma\sigma H_{\text{flop}}}$$

$$\propto \frac{\gamma_{\text{AFM}}}{\omega_{\text{AFM}}}H_{\text{an}}^{\text{AFM}}, \quad \sigma \equiv \frac{\mu_B}{e}\varepsilon P, \quad (1)$$

where γ_{AFM} is the coefficient of internal friction, ω_{AFM} is the antiferromagnetic resonance frequency, H_{flop} is the flop field, M_{AFM} is the absolute value of the AFM local moment, d_{AFM} is the thickness of the AFM layer, γ is the absolute value of the gyromagnetic ratio, $H_{\text{an}}^{\text{AFM}}$ is the anisotropy field of AFM, μ_B is the Bohr magneton, P is the degree of spin polarization, e is the electron charge, and ε is the efficiency of the spin polarization ($\leqslant 1$) [37,38]. For FM, $i_{c,\text{FM}}$ can be expressed as $i_{c,\text{FM}} \propto (\gamma_{\text{AFM}}/\omega_{\text{AFM}})H_{\text{an}}^{\text{FM}}$. In this theory they assume $H_{\text{an}}^{\text{AFM}}$ of ~ 0.1 kOe (e.g., FeMn, IrMn, NiO), and those values are lower than in typical FM, so $i_{c,\text{AFM}}$ is expected to be smaller than $i_{c,\text{FM}}$ [37,38]. Our previous studies demonstrated that the electrical switching of H_{ex} is realized in antiperovskite nitride AFM-Mn$_3$GaN/FM-Co$_3$FeN (001) bilayers with a current

[*]t.hajiri@nagoya-u.jp

density of 1×10^6 A/cm², which is two orders of magnitude smaller than typical FM cases [39]. Towards further understanding, we introduce that the noncollinear AFM antiperovskite manganese nitride Mn_3AN may be a good platform because the AFM magnetic properties, such as the Mn local moment and AFM spin structure (Γ_{4g} and Γ_{5g}), depend on the A atom [40–42].

In this study we prepared fully epitaxial AFM-Mn_3AN/FM-Co_3FeN (001) bilayers with A = Ga, Ni, and $Ni_{0.35}Cu_{0.65}$ (hereinafter referred to as MGN, MNN, and Cu-MNN), which have similar magnetic properties. Shifts in H_{ex} as a function of current density show an exponential change above the threshold current density, regardless of the AFM Mn_3AN layer. We clearly show that the electrical current switching of H_{ex} depends on the AFM local moment of the MAN, even though it has a zero net magnetization. These results highlight that the spin-polarized current has a different degree of action on the AFM local moment depending on its magnitude.

II. EXPERIMENTAL DETAILS

The Mn_3AN (20 nm, bottom)/Co_3FeN (10 nm, top) bilayers (hereinafter referred to as MAN and CFN) were grown using reactive magnetron sputtering on MgO(001) substrates under a total pressure of 2.0 Pa for an Ar + N_2 gas mixture. Details of the film and bilayer growth were reported in our previous works [22,39,43,44]. The crystal structure was analyzed using both in-plane and out-of-plane x-ray diffraction (XRD) measurements with Cu $K\alpha$ radiation. The magnetic properties of the MAN/CFN bilayers were characterized using superconducting quantum interference device (SQUID) magnetometry, and the transport properties were characterized with the standard DC four-terminal method in the current-in-plane configuration with 20-μm-wide Hall bars prepared using conventional photolithographic processes. To induce exchange coupling between the FM and AFM layers, the MAN/CFN bilayers were cooled from 350 to 4 K under an applied magnetic field of +10 kOe along the MAN/CFN [110] direction.

III. RESULTS AND DISCUSSIONS

The out-of-plane and in-plane XRD patterns of the MAN/CFN bilayers are shown in Figs. 1(a) and 1(b), respectively. In Fig. 1(a), only the (00l) MAN and (00l) CFN series exhibit Bragg peaks in the out-of-plane XRD patterns, which indicates the (001)-oriented MAN/CFN bilayers grow well on MgO(001) substrates. In addition, epitaxial growth is confirmed in all MAN/CFN bilayers from the results of the ϕ-scan measurement, as shown in Fig. 1(b), showing that their epitaxial relationship is MgO(001)[100]//MAN(001)[100]//CFN(001)[100].

Figure 2(a) shows the magnetic hysteresis loops for MAN/CFN bilayers measured along the ⟨110⟩ direction at T = 4 K after field cooling (FC). All loops exhibit a clear hysteresis loop shift, indicating the exchange-bias effect appears in all MAN/CFN bilayers. The MAN-layer dependence of the coercive field (H_c) and the exchange-bias field (H_{ex})
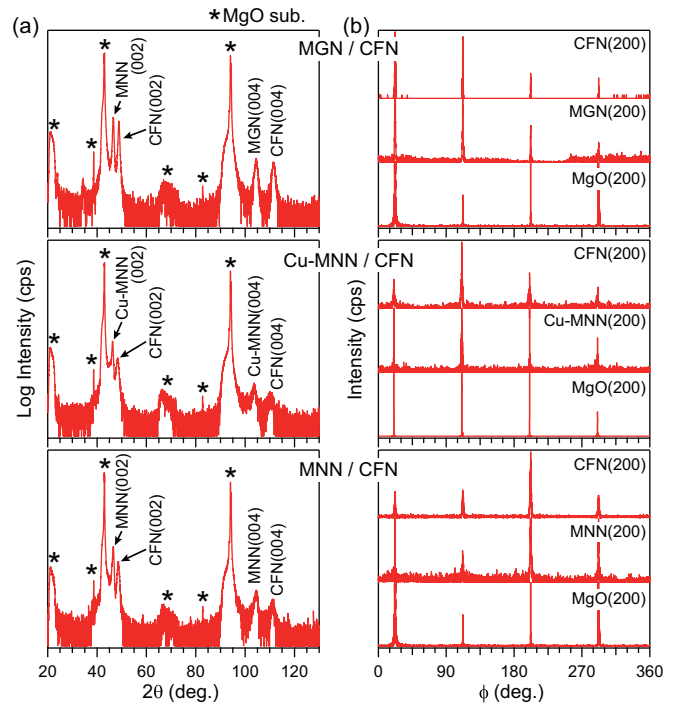

FIG. 1. (a) Out-of-plane and (b) in-plane ϕ scans of the considered MAN/CFN (001) bilayers.

are illustrated in Fig. 2(b). The MAN layer dependence of the anisotropic magnetoresistance (AMR) under an applied magnetic field of 5 kOe after FC is presented in Fig. 2(c). The AMR ratio is defined as AMR = $\{\rho(\theta) - \rho(90°)\}/\rho(90°)$, where θ is the angle between the sensing current parallel to the [110] direction and applied magnetic field in the (001) film plane. Each AMR curve exhibits negative values due to the high polarization of the CFN layer [43,45,46] with no dependence on the rotational direction. In the single-layer CFN films and MGN/CFN bilayers, the AMR ratios are reported to be approximately −0.8% and −0.09%, respectively [39,43].

As summarized in Fig. 2(d), the AMR ratios are similar at approximately −0.1% to −0.2% to the previous MGN/CFN bilayers. Figure 2(e) shows the temperature-dependent resistivity of MAN single-layer films. The Néel temperatures of Cu-MNN and MNN are observed at 190 and 250 K, while that of MGN is higher than 300 K, of which values are consistent from previous reports [22,44,47,48]. Although H_c and H_{ex} show small variations by the MAN layer, no significant exchange-spring effects, such as an enhanced H_c and rotation-direction dependence of AMR [23–25], are observed in each MAN/CFN bilayer. Besides, the resistivity of each MAN single-layer film at T = 4 K is similar at approximately 0.14–0.18 mΩ cm. Thus, these results suggest that each exchange coupling can be compared in electrical switching.

In the electrical current switching for the H_{ex} in MAN/CFN bilayers, Fig. 3(a) shows a microscope image of the MAN/CFN bilayers and experimental configuration. During FC, a magnetic field of 10.0 kOe was applied along the [110] direction. When the pulse current was injected, a magnetic field of $H_{switch} = -5.0$ kOe was applied to define the CFN layer magnetization, which is the opposite of the FC direction.
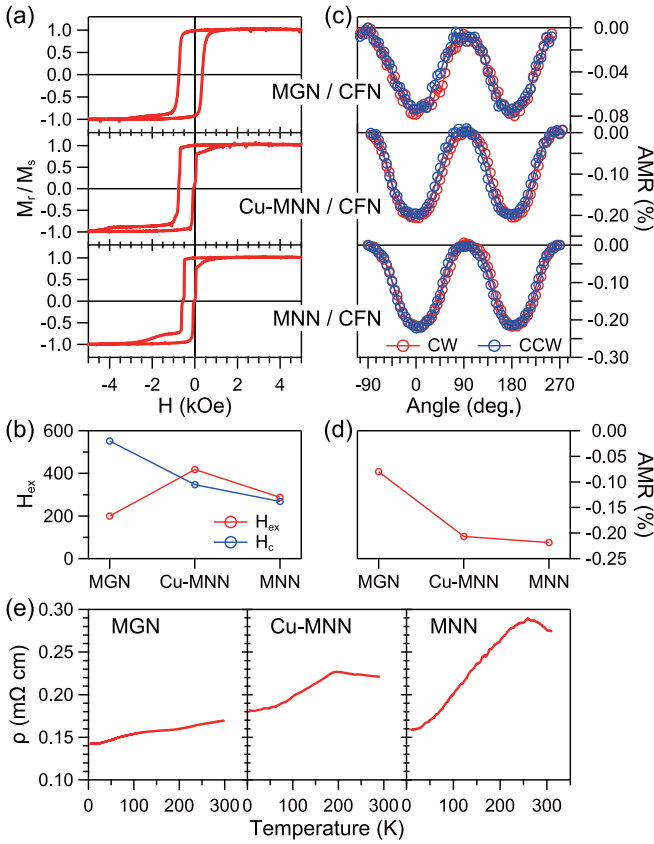
FIG. 2. (a) Magnetic hysteresis loops for the MAN/CFN bilayers at $T = 4$ K after FC. The measurements were performed along the easy axis of CFN $\langle 110 \rangle$. (b) H_c and H_{ex} as functions of the MAN layer. (c) AMR properties of MAN/CFN bilayers, where $0°$ is the sensing current direction parallel to the MAN/CFN[110] direction. The magnetic field of 5 kOe is rotated in the film plane. (d) AMR ratio as a function of the MAN layer. (e) Temperature-dependent resistivity of 50-nm-thick MAN single-layer films.

Before the initial magnetoresistance (MR) measurements after FC was performed, the magnetic field was swept between ± 5.5 kOe several times to avoid the training effect [49]. The MR curves after applying several pulse currents (I_{pulse}) with 100 ms width into the MAN/CFN bilayers are shown in Figs. 3(b)–3(d). Here the current density is calculated from total thickness of each bilayer. In the initial MR curves, the

H_c and H_{ex} obtained from the two MR peaks agree well with those measured using SQUID, as shown in Fig. 2(a), which allows estimating H_{ex} switching from the MR measurements. After applying $I_{\mathrm{pulse}} = 5 \times 10^5$ A/cm^2, the MR peaks shift towards the positive field direction for all MAN/CFN bilayers, indicating that H_{ex} shifts in the opposite direction to the initial H_{ex} as induced from the FC. By increasing I_{pulse}, the shift in H_{ex} gradually increases but with a different saturation behavior. For the MGN/CFN bilayers, the shift in H_{ex} saturates between 5–12×10^5 A/cm^2, while that of Cu-MNN/CFN saturates between 12–19×10^5 A/cm^2. On the other hand, those of the MNN/CFN bilayers continue to shift in the presented MR curves for the I_{pulse} range. We note that the sensing current was set to approximately 5×10^3 A/cm^2, which is sufficiently small for H_{ex} switching. The observed H_{ex} switching is reversible with respect to FM layer magnetization during I_{pulse} injection, as shown in the Supplemental Material Fig. S1 [50] and discussed later.

Figure 4 presents the shifts of H_{ex} normalized by the initial exchange-bias field $H_{ex, ini}$ as a function of I_{pulse}. The shift begins from approximately $I_{\mathrm{pulse}} = 1$–3×10^5 A/cm^2, which is commonly observed. On the other hand, applying an additional I_{pulse} produces different shift behaviors. For MGN, the $H_{ex}/H_{ex, ini}$ curve becomes steeper above 4×10^5 A/cm^2 and saturates at $H_{ex}/H_{ex, ini} = -0.9$ with a saturation current density of $I_{\mathrm{sat.}}$ of 12×10^5 A/cm^2. For Cu-MNN, the $H_{ex}/H_{ex, ini}$ curve analogously becomes steeper at 4×10^5 A/cm^2, but with a smaller slope. The $H_{ex}/H_{ex, ini}$ saturates at -0.55 around 22×10^5 A/cm^2. On the other hand, the MNN linearly changes up to 12×10^5 A/cm^2 and saturates at -0.25 around 28×10^5 A/cm^2. Above 4 or 12×10^5 A/cm^2, the shift of H_{ex} can be fit using the exponential decay function $y = y_0 + Ae^{-(x+x_0)/\tau}$. The decay constants τ for MGN, Cu-MNN, and MNN are 3.42, 6.25, and 8.11×10^5 A/cm^2, respectively. These results indicate that the effects of spin-polarized current on the exchange bias are different between the considered MAN layers. We note that the saturation $H_{ex}/H_{ex, ini}$ depends on the samples, regardless of the MAN layer while the τ does not show a sample dependence, as illustrated in Fig. 9. Generally, the exchange-bias effect is strongly affected by the interface frustration, roughness, and other properties [51,52], which may affect the saturation $H_{ex}/H_{ex, ini}$ and requires future study.

Although it is considered that the torques from the spin-polarized current play an important role in H_{ex} switching as
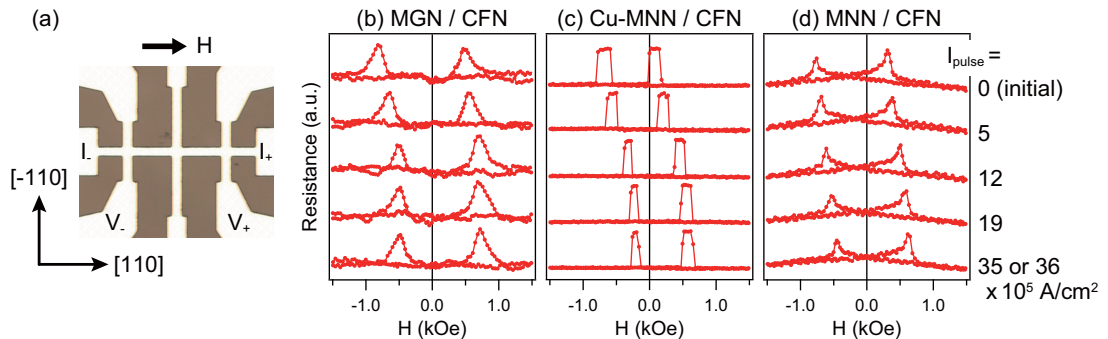

FIG. 3. (a) Microscope image of MAN/CFN bilayers and experimental configuration. (b)–(d) MR curves after applying several 100 ms width pulse currents (I_{pulse}) into the MAN/CFN bilayers. All measurements were performed at $T = 4$ K.
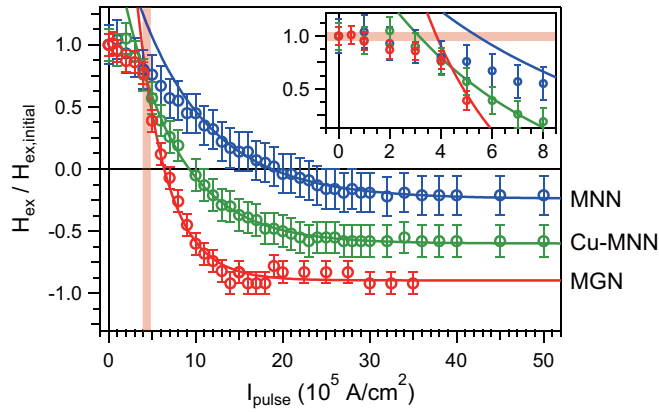
FIG. 4. Shifts of H_{ex} normalized by $H_{ex, ini.}$ as a function of I_{pulse}. The inset shows an enlarged image around $I_{pulse} \sim 8 \times 10^5$ A/cm^2. The bold solid lines are the results of a fit to the exponential decay function $y = y_0 + Ae^{-(x+x_0)/\tau}$.

reported in the previous study [27,28,32–34], to exclude other possible origin, several sequential measurements were performed in Cu-MNN/CFN and MNN/CFN bilayers as shown in Figs. 5(a) and 5(b), respectively. After the initial MR measurements, $I_{pulse} = 50 \times 10^5$ A/cm^2 is injected with 100 ms pulse under -5 kOe (switching process). As discussed in Fig. 3, the MR peaks shift towards the positive field direction. Then I_{pulse} is injected under $+5.0$ kOe (reversing process), and the MR curves return to the initial state with the initial H_{ex}. These results indicate that opposite polarity of H_{ex} also can be manipulated and the CFN layer magnetization with respect to H_{ex} direction plays an important role, probably due to injection of spin-polarized current from CFN layer to MAN layer. In the same manner, switching and reversing processes were sequentially performed with 200 and 400 ms pulse under -5 kOe for switching and 100 ms pulse under $+5$ kOe for reversing. Regardless of the switching pulse width, the H_{ex} after switching shows the same value, and similarly, the H_{ex} after reversing shows the same value as initial H_{ex}, suggesting no sizable difference of thermal effect in these pulse-width range. In addition, $I_{pulse} = \pm 50 \times 10^5$ A/cm^2 was injected with a 100 ms pulse without magnetic field. If significant heating
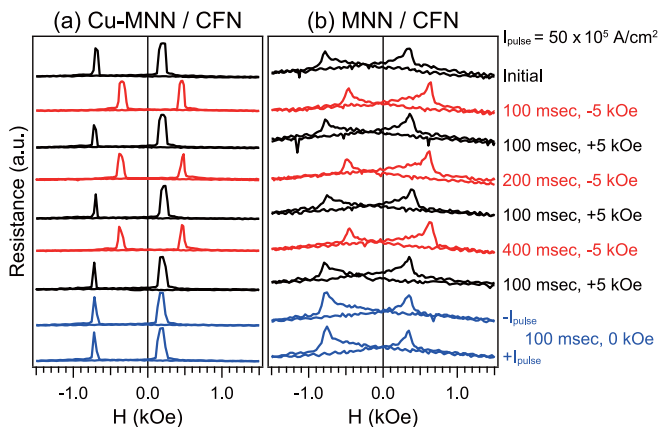

FIG. 5. Sequential switching and reversing results of (a) Cu-MNN/CFN and (b) MNN/CFN bilayers, respectively.
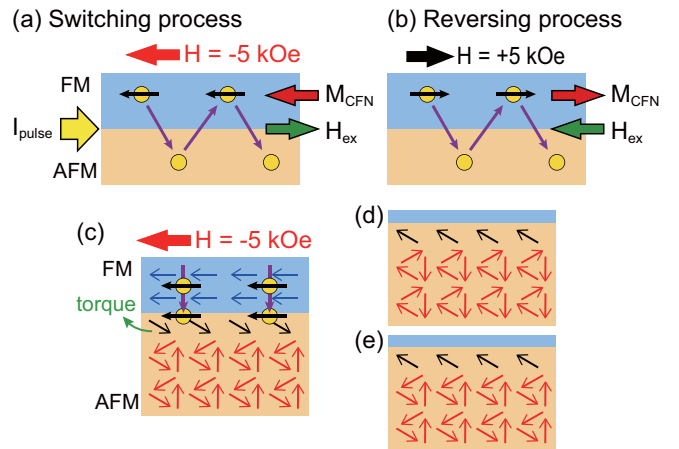

FIG. 6. Schematic illustrations of possible mechanism of H_{ex} switching. (a) Switching process under -5 kOe and (b) reversing process under $+5$ kOe. (c) Enlarged schematic illustration at the interface between FM and AFM. When the current flows from FM to AFM, the current is spin polarized and the spin-polarized current acts (d) only interface uncompensated spins or (e) not only interface uncompensated spins, but also to a certain depth of bulk AFM spins.

and subsequent cooling process occur by I_{pulse}, the exchange-coupling properties are expected to be affected when there is no magnetic field. However, no sizable difference by applying $\pm I_{pulse}$ is observed in not only the magnitude of H_{ex} but also shape of MR curves in both Cu-MNN/CFN and MNN/CFN bilayers. Besides, the temperature increase during a 100 ms pulse duration was measured as shown in the Supplemental Material Fig. S2 [50]. The temperature reached until the H_{ex} switching is completed is sufficiently lower than the Néel temperature. From these results we conclude that most switching effect comes from spin-polarized current rather than thermal effect.

The schematic illustration of possible H_{ex} switching mechanism are presented in Fig. 6. Since the resistivity of CFN is similar at around 0.1 mΩ cm with each MAN layer, here we assume that current can flow back and forth between FM and AFM as illustrated in Figs. 6(a) and 6(b). When the current flows from CFN to MAN, the current is spin polarized due to CFN spin polarization and its polarized direction can be directed in the opposite direction to H_{ex} by the magnetic field as illustrated in Figs. 6(a)–6(c). The previous study argued that the spin-polarized current induces torques on interface uncompensated spins as illustrated in Fig. 6(d). On the other hand, resent SOT studies of noncollinear AFM Mn$_3$Sn demonstrate the manipulation of AFM moments even at 40-nm-thick films [17]. Hence, as illustrated in Fig. 6(e), the spin-polarized current may be able to act not only on interface uncompensated spins but also to a certain depth of bulk AFM spins. Although it is difficult to distinguish between these two possible pictures in this study, in the discussion below we assume that interface AFM spins which cause H_{ex} keep the bulk AFM properties, such as the local moment of the AFM magnetic atoms, the anisotropy of the AFM, and the AFM Néel vector.

Finally, we would like to discuss the different H_{ex} switching behaviors. According to theoretical studies of STT
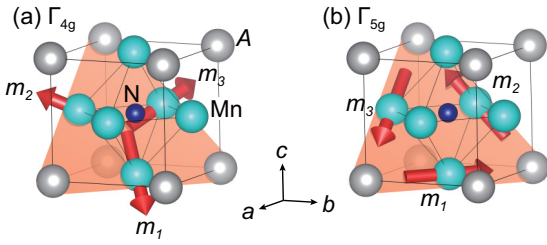
FIG. 7. (a) Γ_{4g} and (b) Γ_{5g} AFM spin structures visualized using VESTA package [54].

in AFM materials, the critical current is affected by the local moment of the AFM magnetic atoms, the anisotropy of the AFM, and the relative angle between the injected spin direction and the AFM Néel vector [37,38,53]. In MAN systems, the AFM spin orders (Γ_{4g} and Γ_{5g}, shown in Fig. 7) vary depending on the composition of the A site; Γ_{5g} is observed in MGN and MNN and Γ_{4g} in Cu-MNN. In such noncollinear AFMs with triangular magnetic configurations composed of three equivalent magnetic directions ($\boldsymbol{m}_1$, $\boldsymbol{m}_2$, and $\boldsymbol{m}_3$, shown in Fig. 7), the AFM Néel vectors can be expressed using two vectors $\boldsymbol{L}_1$ and $\boldsymbol{L}_2$ as [55]

$$\boldsymbol{L}_1 = \boldsymbol{m}_1 + \boldsymbol{m}_2 - 2\boldsymbol{m}_3,$$
$$\boldsymbol{L}_2 = \sqrt{3}(\boldsymbol{m}_1 - \boldsymbol{m}_2). \tag{2}$$

A theoretic study indicates that the torque efficiency is proportional to $\sin\theta$, where θ is the relative angle between the injected spin direction and the AFM Néel vector [53]. In this study, the injected spin direction from the FM CFN layer is $\langle 110 \rangle$ as determined from the external magnetic field. The relative angles between $\boldsymbol{L}_1$, $\boldsymbol{L}_2$ and $\langle 110 \rangle$ are summarized in Table I. From the perspective of $\sin\theta$, there is no difference between Γ_{4g} and Γ_{5g} orders. Therefore, we conclude that the effect of the relative angle between the injected spin direction and the AFM Néel vector is relatively small.

On the other hand, although there are no reports on the actual magnetocrystalline anisotropy in MAN systems, it is reported that the Mn moments of Cu-MNN begin to cant in the (111) plane when a magnetic field is applied along the $[-1-12]$ direction with a magnitude that is larger than the threshold value [44]. Thus, epitaxial-grown MAN(111) films are prepared [22,44] and compared to the magnetization loop along the $[-1-12]$ direction for each MAN(111) film as shown in Fig. 8. All MAN (111) films show the similar in-plane magnetization behavior with a threshold value of 1 T, indicating that these AFM materials have similar anisotropies, at least for canting in the (111) plane. Therefore, it is con-

TABLE I. Relative angles between the AFM Néel vectors ($\boldsymbol{L}_1$, $\boldsymbol{L}_2$) and the $\langle 110 \rangle$ direction for Γ_{4g} and Γ_{5g} AFM orders.

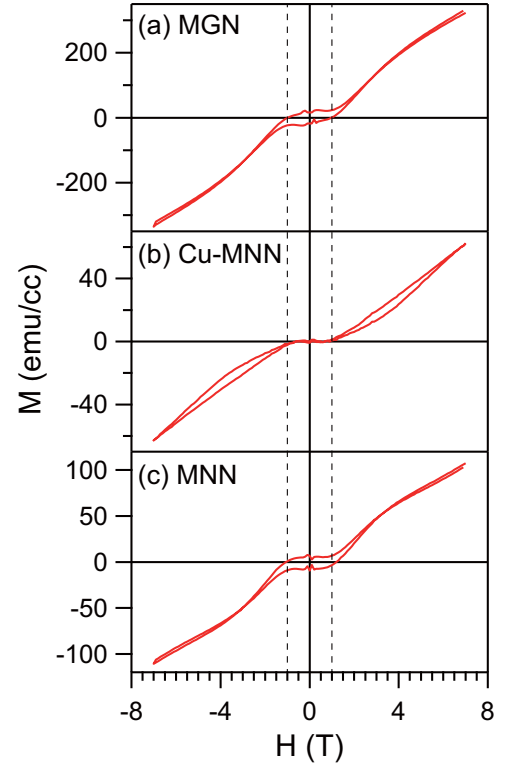| AFM order		$\boldsymbol{L}_1$	$\boldsymbol{L}_2$	Average
Γ_{4g}	θ	73°	60°	–
	$\sin\theta$	0.96	0.87	0.91
Γ_{5g}	θ	60°	107°	–
	$\sin\theta$	0.87	0.96	0.91

FIG. 8. In-plane magnetic hysteresis loops for (a) MGN, (b) Cu-MNN, and (c) MNN (111) films measured at $T = 4$ K. The magnetic field is applied along the $[-1-12]$ direction.

sidered that the effects of both the relative angle between the injected spin direction and the AFM Néel vector and the anisotropy are small.

In MAN systems, the Mn local moment is known to depend on the A atom and is proportional to the number of electrons outside of the Ar closed shells [40]. From theoretical calculations [41], the Mn local moments for MGN and MNN are 2.43 and 2.83 μ_B/Mn atom, respectively, and that of Cu-MNN is estimated as 2.74 μ_B/Mn atom. Figure 9 compares the decay constant τ and saturation current $I_{\text{sat.}}$ as a functions of the Mn local moments for MAN, indicating that both the τ and $I_{\text{sat.}}$ increase with Mn local moments of MAN. Although $I_{\text{sat.}}$ shows certain sample dependence probably due to the interface condition, even taking into account those variations, the estimated linear relationship seems to be valid. This conclusion can be reinforced by τ because it shows a small sample dependence.

In addition, to check the universality of this relationship, we considered collinear AFM MnN/CFN bilayers, because the MnN has a rocksalt structure with a much higher Néel temperature at 650 K and larger AFM local moment of 3.3 μ_B/Mn than for MAN [56–58]. As shown in Fig. S3 [50], the $H_{\text{ex}}/H_{\text{ex,ini}}$ shifts with respect to I_{pulse} in the same manner, and $I_{\text{sat.}}$ as a function of the Mn local moment follows an almost proportional relationship. These results indicate that the spin-polarized current has a different degree of action on the AFM local moment depending on its magnitude. The linear fitting line intersects the x axis in the vicinity of 2 μ_B/Mn. Since a scaling is not expected to be achieved for
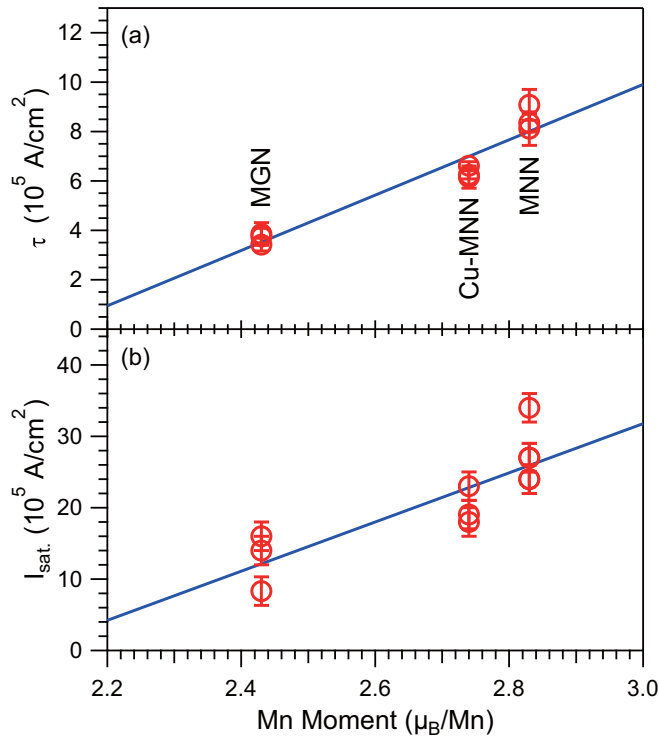
FIG. 9. (a) Decay constants τ and (b) $I_{sat.}$ as functions of the Mn moment for Mn$_3$AN. The bold solid lines are linear fits.

the local moments of less than $2\mu_B$/atom, switching experiments with such AFMs are of interest. Typical AFMs used in spintronics such as MnIr and MnPt, however, exhibit large local magnetic moments of 3–4 μ_B/Mn. Another possibility

would be a double helical AFM MnP [59] and CrAs [60], which have 1.3 μ_B/Mn and 1.7 μ_B/Cr, respectively, and it is worthy of future research on those AFM switching. We note that the similar order of switching current density has been recently realized in the SOT of noncollinear AFM of MGN (2.43 μ_B/Mn) and Mn$_3$Sn (3.2 μ_B/Mn [61]) with 1.5 and 5×10^6 A/cm^2, respectively [16,17]. Since STT consumes more energy than SOT in traditional STT and SOT of FM [62], our results may imply that SOT in such AFMs has a great potential to realize even lower current density switching.

In contrast to the well-studied FM STT, while there are several reports on the electrical manipulation of AFM moments, there is no systematic study demonstrated to date. This is because it is difficult to read out AFM moments electrically. As the exchange bias generally appears at the interface between FM and AFM regardless of material combination, our results offer further experiments and may provide a deeper understanding of the electrical manipulation of AFM moments.

[1] J. A. Katine, F. J. Albert, R. A. Buhrman, E. B. Myers, and D. C. Ralph, Phys. Rev. Lett. **84**, 3149 (2000).

[2] A. Fert, V. Cros, J.-M. George, J. Grollier, H. Jaffrés, A. Hamzic, A. Vaurés, G. Faini, J. Ben Youssef, and H. Le Gall, J. Magn. Magn. Mater. **272**, 1706 (2004).

[3] I. M. Miron, G. Gaudin, S. Auffret, B. Rodmacq, A. Schuhl, S. Pizzini, J. Vogel, and P. Gambardella, Nat. Mater. **9**, 230 (2010).

[4] L. Liu, C.-F. Pai, Y. Li, H. W. Tseng, D. C. Ralph, and R. A. Buhrman, Science **336**, 555 (2012).

[5] T. Jungwirth, X. Martí, P. Wadleyand, and J. Wunderlich, Nat. Nanotechnol. **11**, 231 (2016).

[6] V. Baltz, A. Manchon, M. Tsoi, T. Moriyama, T. Ono, and Y. Tserkovnyak, Rev. Mod. Phys. **90**, 015005 (2018).

[7] C. Song, Y. You, X. Chen, X. Zhou, Y. Wang, and F. Pan, Nanotechnology **29**, 112001 (2018).

[8] P. Wadley, B. Howells, J. Železný, C. Andrews, V. Hills, R. P. Campion, V. Novák, K. Olejník, F. Maccherozzi, S. S. Dhesi, S. Y. Martin, T. Wagner, J. Wunderlich, F. Freimuth, Y. Mokrousov, J. Kuneš, J. S. Chauhan, M. J. Grzybowski, A. W. Rushforth, K. W. Edmonds, B. L. Gallagher, and T. Jungwirth, Science **351**, 587 (2016).

[9] T. Matalla-Wagner, M.-F. Rath, D. Graulich, J.-M. Schmalhorst, G. Reiss, and M. Meinert, Phys. Rev. Appl. **12**, 064003 (2019).

[10] S. Y. Bodnar, L. Šmejkal, I. Turek, T. Jungwirth, O. Gomonay, J. Sinova, A. A. Sapozhnik, H. J. Elmers, M. Kläui, and M. Jourdan, Nat. Commun. **9**, 348 (2018).

[11] M. Meinert, D. Graulich, and T. Matalla-Wagner, Phys. Rev. Appl. **9**, 064040 (2018).

[12] X. Z. Chen, R. Zarzuela, J. Zhang, C. Song, X. F. Zhou, G. Y. Shi, F. Li, H. A. Zhou, W. J. Jiang, F. Pan, and Y. Tserkovnyak, Phys. Rev. Lett. **120**, 207204 (2018).

[13] L. Baldrati, O. Gomonay, A. Ross, M. Filianina, R. Lebrun, R. Ramos, C. Leveille, F. Fuhrmann, T. R. Forrest, F. Maccherozzi, S. Valencia, F. Kronast, E. Saitoh, J. Sinova, and M. Kläui, Phys. Rev. Lett. **123**, 177201 (2019).

[14] T. Moriyama, K. Oda, and T. Ono, Sci. Rep. **8**, 14167 (2018).

[15] Y. Cheng, S. Yu, M. Zhu, J. Hwang, and F. Yang, Phys. Rev. Lett. **124**, 027202 (2020).

[16] T. Hajiri, S. Ishino, K. Matsuura, and H. Asano, Appl. Phys. Lett. **115**, 052403 (2019).

[17] H. Tsai, T. Higo, K. Kondou, T. Nomoto, A. Sakai, A. Kobayashi, T. Nakano, K. Yakushiji, R. Arita, S. Miwa, Y. Otani, and S. Nakatsuji, Nature (London) **580**, 608 (2020).

[18] R. Mishra, J. Yu, X. Qiu, M. Motapothula, T. Venkatesan, and H. Yang, Phys. Rev. Lett. **118**, 167201 (2017).

[19] J. Finley and L. Liu, Phys. Rev. Appl. **6**, 054001 (2016).

[20] S. Nakatsuji, N. Kiyohara, and T. Higo, Nature (London) **527**, 212 (2015).

[21] Z. Liu, H. Chen, J. Wang, J. Liu, K. Wang, Z. Feng, H. Yan, X. Wang, C. Jiang, J. Coey, and A. H. MacDonald, Nat. Electron. **1**, 172 (2018).

[22] K. Zhao, T. Hajiri, H. Chen, R. Miki, H. Asano, and P. Gegenwart, Phys. Rev. B **100**, 045109 (2019).

[23] B. G. Park, J. Wunderlich, X. Martí, V. Holý, Y. Kurosaki, M. Yamada, H. Yamamoto, A. Nishide, J. Hayakawa, H. Takahashi, A. B. Shick, and T. Jungwirth, Nat. Mater. **10**, 347 (2011).

[24] X. Martí, B. G. Park, J. Wunderlich, H. Reichlová, Y. Kurosaki, M. Yamada, H. Yamamoto, A. Nishide, J. Hayakawa, H. Takahashi, and T. Jungwirth, Phys. Rev. Lett. **108**, 017201 (2012).

[25] T. Hajiri, M. Matsushita, Y. Z. Ni, and H. Asano, Phys. Rev. B **95**, 134413 (2017).

[26] Y. Y. Wang, C. Song, B. Cui, G. Y. Wang, F. Zeng, and F. Pan, Phys. Rev. Lett. **109**, 137201 (2012).

[27] Z. Wei, A. Sharma, A. S. Nunez, P. M. Haney, R. A. Duine, J. Bass, A. H. MacDonald, and M. Tsoi, Phys. Rev. Lett. **98**, 116603 (2007).

[28] X.-L. Tang, H.-W. Zhang, H. Su, Z.-Y. Zhong, and Y.-L. Jing, Appl. Phys. Lett. **91**, 122504 (2007).

[29] S. A. Wolf, D. D. Awschalom, R. A. Buhrman, J. M. Daughton, S. von Molnár, M. L. Roukes, A. Y. Chtchelkanova, and D. M. Treger, Science **294**, 1488 (2001).

[30] J. Åkerman, Science **308**, 508 (2005).

[31] F. Radu and H. Zabel, *Magnetic Heterostructures* (Springer, Berlin, 2008).

[32] X. L. Tang, H. W. Zhang, H. Su, Y. L. Jing, and Z. Y. Zhong, J. Appl. Phys. **105**, 073914 (2009).

[33] X. L. Tang, H. W. Zhang, H. Su, Y. L. Jing, and Z. Y. Zhong, Phys. Rev. B **81**, 052401 (2010).

[34] J. Guo, M. B. A. Jalil, and S. Ghee, J. Appl. Phys. **109**, 07C915 (2011).

[35] P.-H. Lin, B.-Y. Yang, M.-H. Tsai, P.-C. Chen, K.-F. Huang, H.-H. Lin, and C.-H. Lai, Nat. Mater. **18**, 335 (2019).

[36] Y. Wang, X. Zhou, C. Song, Y. Yan, S. Zhou, G. Wang, C. Chen, F. Zeng, and F. Pan, Adv. Mater. **27**, 3196 (2015).

[37] H. V. Gomonay and V. M. Loktev, Low Temp. **40**, 17 (2014).

[38] H. V. Gomonay and V. M. Loktev, Phys. Rev. B **81**, 144427 (2010).

[39] H. Sakakibara, H. Ando, Y. Kuroki, S. Kawai, K. Ueda, and H. Asano, J. Appl. Phys. **117**, 17D725 (2015).

[40] D. Fruchart and E. F. Bertaut, J. Phys. Soc. Jpn. **44**, 781 (1978).

[41] J. Zemen, Z. Gercsi, and K. G. Sandeman, Phys. Rev. B **96**, 024451 (2017).

[42] Vu Thi Ngoc Huyen, M. T. Suzuki, K. Yamauchi, and T. Oguchi, Phys. Rev. B **100**, 094426 (2019).

[43] H. Sakakibara, H. Ando, T. Miyawaki, K. Ueda, and H. Asano, IEEE Trans. Magn. **50**, 2600404 (2014).

[44] R. Miki, K. Zhao, T. Hajiri, P. Gegenwart, and H. Asano, J. Appl. Phys. **127**, 113907 (2020).

[45] Y. Takahashi, Y. Imai, and T. Kumagai, J. Magn. Magn. Mater. **323**, 2941 (2011).

[46] Y. Sakuraba, S. Kokado, Y. Hirayama, T. Furubayashi, H. Sukegawa, S. Li, Y. K. Takahashi, and K. Hono, Appl. Phys. Lett. **104**, 172407 (2014).

[47] W. J. Feng, D. Li, Y. F. Dend, Q. Zhang, and H. H. Zhang, J. Mater. Sci. **45**, 2770 (2010).

[48] D. Kasugai, A. Ozawa, T. Inagaki, and K. Takenaka, J. Appl. Phys. **111**, 07E314 (2012).

[49] S. Polisetty, S. Sahoo, and C. Binek, Phys. Rev. B **76**, 184423 (2007).

[50] See Supplemental Material at http://link.aps.org/supplemental/10.1103/PhysRevB.102.014404 for additional details about the reversible H_{ex} switching with respect to FM layer magnetization during pulse current injection, the pulse current induced joule heating, and H_{ex} switching on MnN/CFN bilayers.

[51] E. Jiménez, J. Camarero, J. Sort, J. Nogués, N. Mikuszeit, J. M. García-Martín, A. Hoffmann, B. Dieny, and R. Miranda, Phys. Rev. B **80**, 014415 (2009).

[52] M. Vafaee, S. Finizio, H. Deniz, D. Hesse, H. Zabel, G. Jakob, and M. Kläui, Appl. Phys. Lett. **108**, 072401 (2016).

[53] A. S. Núñez, R. A. Duine, Paul Haney, and A. H. MacDonald, Phys. Rev. B **73**, 214426 (2006).

[54] K. Homma and F. Izumi, J. Appl. Crystallogr. **44**, 1272 (2011).

[55] H. V. Gomonay, Roman V. Kunitsyn, and Vadim M. Loktev, Phys. Rev. B **85**, 134446 (2012).

[56] K. Suzuki, Y. Yamaguchi, T. Kaneko, H. Yoshida, Y. Obi, H. Fujimori, and H. Morita, J. Phys. Soc. Jpn. **70**, 1084 (2001).

[57] T. Hajiri, T. Yoshida, M. Filianina, S. Jaiswal, B. Borie, H. Asano, H. Zabel, and M. Kläui, J. Phys.: Condens. Matter **30**, 015806 (2017).

[58] T. Hajiri, T. Yoshida, S. Jaiswal, M. Filianina, B. Borie, H. Ando, H. Asano, H. Zabel, and M. Kläui, Phys. Rev. B **94**, 184412 (2016).

[59] Z. Gercsi and K. G. Sandeman, Phys. Rev. B **81**, 224426 (2010).

[60] H. Boller and A. Kallel, Solid State Commun. **9**, 1699 (1971).

[61] H. Yang, H. Sun, Y. Zhang, W.-J. Sh, S. S. P. Parkin, and B. Yan, New J. Phys. **19**, 015008 (2017).

[62] K. Jabeur, G. D. Pendina, and G. Prenat, Electr. Electron. Eng. Int. J. **6**, 1 (2017).